Scanning performances of wideband connected arrays in the presence of a backing reflector

Scanning Performances of Wideband Connected Arrays in the Presence of a Backing Reflector

Andrea Neto, *Member, IEEE*, Daniele Cavallo, *Student Member, IEEE*, Giampiero Gerini, *Senior Member, IEEE*, and Giovanni Toso, *Senior Member, IEEE*

***Abstract*—In this paper, the scanning performances of connected arrays that include backing reflectors are investigated. The comparison between connected dipoles and slots is based on the properties of the corresponding Green's functions (GFs). The investigation reveals that connected arrays of dipoles are better suited to scan to wide angles (45°), retaining the minimal number of transmit/receive (T/R) modules. This paper quantifies and motivates this preference. Eventually, the theoretical design of a fully efficient, 40% bandwidth (BW), planar array with the lowest possible cross polarization is presented.**

***Index Terms*—Antenna arrays, cross polarization, Green's function (GF), ultrawideband antennas.**

I. Introduction

A NUMBER of applications have been recently arising that require antennas with high directivity, wide bandwidth (BW), low profile, low cross polarization, and electronic beam scanning. These applications range from multifunction defense and security radars in X-band and lower, to communication applications in Ku-bands, from earth-based deep space investigation (e.g., square kilometer array [1]), to satellite based submillimeter (sub-mm) wave instruments (e.g., SPICA [2]). Connected arrays are now considered as one of the most promising antenna solutions for such applications. While their origin stems from the concept of self complementarity [3], [4], recently, it was Hansen [5] that brought the concept of connected arrays of dipoles to the attention of the antenna community. A detailed study of finite array of dipoles connected end-to-end by reactive loads was presented in [6]. Such investigation showed that non-Foster coupling between contiguous elements allows optimizing the performance over a decade BW. The design strategy for arrays of disconnected dipoles presented in [7], while appearing radically different because it is based on capacitively loaded dipoles, presents some similarities with the one based on connected arrays. Indeed, the purpose and effect of the capacitive loading in [7] is to obtain almost continuous currents among the different dipole elements, thus realizing the continuous sheet current from Wheeler [8]. This is the same scope of the connected dipole arrays. In [9], the connected dipole concept was extended to the dual structure, based on slots. In [10] and [11], Green's function (GF) of such long slot arrays was derived and presented in analytical form, for both finite and infinite arrays, starting from a spectral representation of the field in each slot [12]. Recently, other authors [13] have been investigating the GF of connected array structures with full-wave techniques, obtaining models which also include the details of the feeding structures. The availability of GF greatly facilitates the design steps and eventually the first functioning demonstration of a planar connected array was presented in [14]. This consisted of a 4×8 connected array of slots, with a backing reflector, radiating at broadside with reasonable efficiency, on a BW that spanned from 150 to 650 MHz.

In this paper, the properties of connected slots and dipoles are investigated and compared, focusing, for the first time, on the array scanning properties. The dependence of the performances of this type of arrays on a number of factors like the array sampling, the distance of the radiating aperture from the ground plane, and the energy stored in the feeding points is analyzed and described in detail. In particular, it is shown how the capacitive energy stored in the feeding gaps of a connected dipole structure can be used to match the array for wide scanning angles. This finding sets a preference for connected dipoles over connected slots. A design with a BW in the order of 40% and wide sampling periods ($d_x = d_y \approx 0.5\lambda_0$ at the highest useful frequency) is presented and discussed, showing its full functionality also when scanning up to $\pm 45^\circ$.

The radiation patterns of such an 8×8 finite array are investigated using the appropriate analytical expressions for the far-field co- and cross-polarized directivities. These expressions are derived directly from the GF and thus remain valid even for a small connected array. On the contrary, the very widely used approximations based on infinite-array theory [15] and consequent windowing [16], although very efficient from the computational point of view, would fail in equivalently small array cases. This is because of the intrinsic nature of connected arrays: they are characterized by a strong mutual coupling which does not allow neglecting global array effects. Eventually, the low-cross-polarization level when scanning in the diagonal plane is highlighted as the main characterizing feature of these broadband arrays.

The findings of this paper constitute the basis for a prototype that is presently being manufactured and will be the object of a future publication.

Manuscript received September 23, 2008; revised March 30, 2009. First published July 28, 2009; current version published October 07, 2009. This work was supported by the European Space Agency "Advanced Antenna Concepts for Aircraft in Flight Entertainment" under Estec Contract C19865, and by the TNO internal Radar Program for the Dutch Royal Navy.

A. Neto is with TNO, Defense, Security and Safety, 2597 AK Den Haag, The Netherlands (e-mail: andrea.neto@tno.nl).

D. Cavallo and G. Gerini are with TNO, Defense, Security and Safety, 2597 AK Den Haag, The Netherlands and also with the Eindhoven University of Technology, 5612 AZ Eindhoven, The Netherlands (e-mail: daniele.cavallo@tno.nl; giampiero.gerini@tno.nl).

G. Toso is with the Electromagnetics Division, European Space Agency, 2200 AG Noordwijk, The Netherlands (e-mail: Giovanni.Toso@esa.int).

Digital Object Identifier 10.1109/TAP.2009.2028631

II. Impedance of Connected Arrays

The geometries of the slot and dipole arrays that we consider are shown in Fig. 1(a) and (b), respectively, together with the pertinent reference system and characterizing parameters. The GF of an array of long slots periodically fed, in the presence of a backing reflector, was derived in [11]. From the GF, the input impedance was also derived, which can be explicitly expressed as follows:

$$z^{br}_{\rm slot} = \frac{k_0\zeta_0 d_y}{d_x}\sum_{m_x=-\infty}^{\infty}\mathrm{sinc}^2(k_{xm}\delta_s/2) \cdot \frac{1}{(k_0^2-k_{xm}^2)\sum\limits_{m_y=-\infty}^{\infty}\dfrac{J_0\left(k_{ym}\dfrac{w_s}{2}\right)(1-j\cot(k_{zm}h_s))}{k_{zm}}} \quad (1)$$

where J_0 is the Bessel function of zeroth order, k_0 is the free-space propagation constant, $k_{xm} = k_0\sin\theta\cos\phi - (2\pi m_x)/(d_x)$, $k_{ym} = k_0\sin\theta\sin\phi - (2\pi m_y)/(d_y)$, and $k_{zm} = \sqrt{k_0^2 - k_{xm}^2 - k_{ym}^2}$. For the dipole structure, with backing reflector as in Fig. 1(b), the GF can be evaluated once the electric current on a single infinitely extended dipole fed by a δ-gap voltage source is known. The derivation of this current is shown in (19) in the Appendix. The extension to an infinite periodic array of dipoles periodically fed is obtained extending the procedure shown in [11]. Eventually, the following expression for the active input admittance at each feed can be written as:

$$y^{br}_{\rm dipole} = \frac{k_0 d_y}{\zeta_0 d_x}\sum_{m_x=-\infty}^{\infty}\mathrm{sinc}^2(k_{xm}\delta_d/2) \cdot \frac{1}{(k_0^2-k_{xm}^2)\sum\limits_{m_y=-\infty}^{\infty}\dfrac{J_0\left(k_{ym}\dfrac{w_d}{2}\right)}{k_{zm}(1-j\cot(k_{zm}h_d))}}. \quad (2)$$

Note that here it is assumed that the electric dipoles [Fig. 1(b)] are oriented along x, implying that the connected array of dipoles operates in a polarization orthogonal to the one associated with the connected array of slots in Fig. 1(a).

A. Dominant Floquet Wave

Both expressions (1) and (2) present a clear resonance condition. The condition can be gathered by considering only the first mode $m_x = m_y = 0$ in the double summations. Note that the dominant mode representation is a realistic hypothesis only when the array is extremely well sampled. The slot array impedance becomes

$$z^{br}_{\rm slot} = \frac{\zeta_0 d_y}{d_x}\frac{\cos\theta}{(1-\sin^2\theta\cos^2\phi)(1-j\cot(k_0 h_s\cos\theta))}. \quad (3)$$

The resonance of the impedance in (3) is clearly given by the condition $k_0 h_s\cos\theta = \pi/2$, which implies $h_s = \lambda_0/4$ for broadside radiation. In this case, $z^{br}_{\rm slot} = (\zeta_0 d_y/d_x)$, which is twice as large as the asymptotic value for low frequency of a connected array of slots without backing reflector $z^{br}_{\rm slot} \to 2z_{\rm slot}$. The factor 2 derives from the fact that, with a backing reflector, all the power provided to the array radiating aperture is radiated in the upper half space.

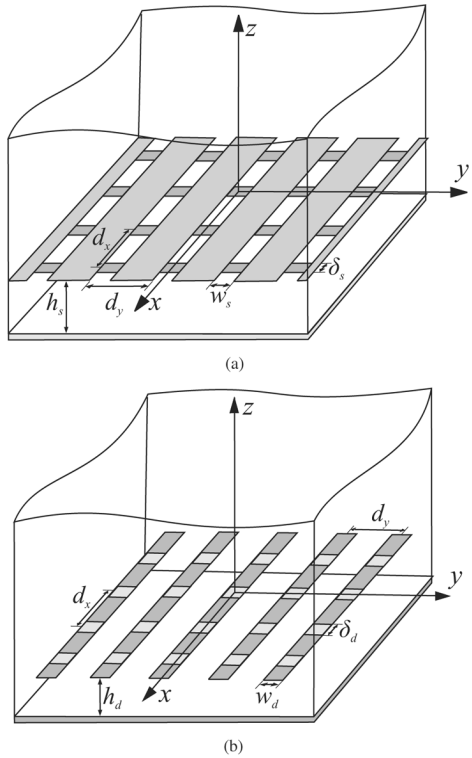

Fig. 1. Geometries of 2-D connected arrays of (a) slots and (b) dipoles with backing reflector.

Also for the dipole case, retaining only the dominant mode, one obtains an expression extremely similar to the one in (3)

$$z^{br}_{\rm dipole} = \frac{\zeta_0 d_x}{d_y}\frac{1-\sin^2\theta\cos^2\phi}{\cos\theta(1-j\cot(k_0 h_d\cos\theta))}. \quad (4)$$

The only difference with respect to (3) resides in the changed ϕ-dependence, congruent with the fact that the E- and H-planes are inverted in the dipole configuration. This implies that no major differences can be observed, as far as the BWs of connected dipoles and slots are concerned.

For any given θ or ϕ, (3) and (4) state that the array can be matched with a real transmission line to present a reflection coefficient lower than -10 dB over about a 60% relative BW. The transmission lines characteristic impedance that guarantees the widest frequency BW is the one associated with the matching condition at broadside (377 Ω).

The most important impact on the matching of the arrays as a function of the scanning derives from the variation of the resonance frequency. As the scanning angle grows, as an example to 45°, the electrical length $(k_0 h_s\cos\theta)$ becomes smaller. This implies that the resonance condition is achieved for frequency 30% higher with respect to broadside.

Thus, simplifying, the maximum possible overlap between the matching BW achieved at broadside and at 45° scanning, on both planes, is about 30%. An example of this behavior is shown in Fig. 2 where the reflection coefficient, with respect to a 400-Ω transmission line, of a well-sampled array is shown. The periods of the array are $d_x = d_y = 0.4\lambda_0$, where $\lambda_0 = (c_0/f_0)$

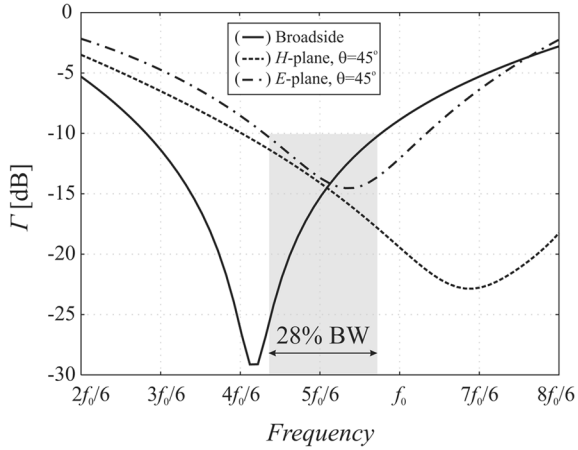

Fig. 2. Active reflection coefficient, with respect to a 400-Ω, of a slot array characterized by $d_x = d_y = 0.4\lambda_0$, $w_s = \delta_s = 0.2\lambda_0$, and $h_s = 0.31\lambda_0$, scanning at broadside and toward $\theta = 45°$ in the two main planes.

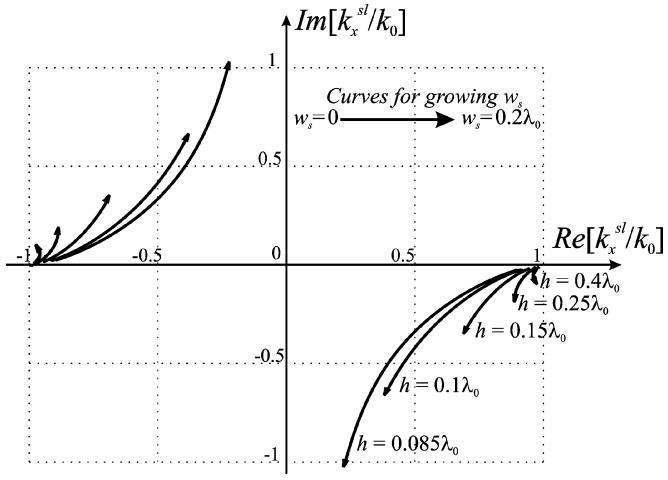

Fig. 3. Polar singularities in the complex k_x/k_0 plane when the array is pointing broadside. The dimensions are $d_x = d_y = 0.5\lambda_0, \delta_s = 0.1\lambda_0$, while w_s and h_s are varying.

and c_0 is the free-space speed of light, and the curves are plotted as a function of the frequency, normalized with respect to f_0. The results are shown for the cases of scanning at broadside and toward $\theta = 45°$, in the two main planes. The curves are obtained implementing the full expression in (1).

Note that similar considerations were already observed for resonant dipole structures from [17]. However, here these properties have been rigorously demonstrated using the GF of the structure.

The results shown in Fig. 2 highlight two drawbacks. The first is that the achieved BW is large, 28%, but not very large. The second is that at the highest frequency of operation the array is highly sampled, which would imply a very high number of transmit/receive (T/R) modules in a large array. The aim of this paper is to identify a structure that, while maximizing the BW (aiming at 40%) for wide scanning, also minimizes the number of T/R modules.

III. Analysis of Polar Singularities of the Longitudinal Spectra

In this section, we discuss the feasibility of reducing the distance between the radiating elements and the backing reflector h_s or h_d, in order to shift the operational BW of the array at higher frequency, while maintaining the same sampling period. Normally, the infinite-array analysis is used for the bulk dimensioning of the array, while one proceeds to finite-array analysis, via explicit introduction of the mutual coupling concept, only for the fine tuning. This approach is valid also with connected arrays. However, the connection of the different feeds implies that the propagation of waves along the longitudinal direction of the slots or dipoles, $\mathbf{i}_x$ in both cases (Fig. 1), strongly influences also the infinite-array behavior. Here we will discuss the nature of these propagations highlighting the main differences between connected slots and dipoles.

A. Leaky Wave Poles in Connected Slots

A parallel plate waveguide is compatible with a transverse electromagnetic (TEM) guided mode. This mode, when perturbed by the presence of periodic slots, originates leaky waves which radiate power in unwanted directions. Accordingly, connected arrays of slots backed by a ground plane [Fig. 1(a)] can support leaky waves. To investigate the properties of such leaky waves, one must study their propagation along the slots. At this aim, it is necessary to do one step back and consider each of the slots in the array, as if it were excited by only one feed. In that case, the representation of the voltage along each slot would be obtained as an inverse integral in k_x, by using [11, eq. (1) and (18)]. Note that in the present case, (18) in [11] is the kernel of the m_x summation in (1).

We will concentrate the attention to the case in which the array is phased to radiate toward $\phi = 0$ (so that $k_{y0} = k_0 \sin\theta \sin\phi = 0$) and we will investigate the spectrum in k_x. Expected branch point singularities appear in $\pm k_0$. However, also polar singularities emerge as solutions of the dispersion equation that is obtained equating to zero the denominator in (1)

$$\left(k_0^2 - k_x^2\right) \sum_{m_y=-\infty}^{\infty} \frac{J_0\left(k_{ym}\frac{w_s}{2}\right)\left(1 - j\cot(k_{zm}h_s)\right)}{k_{zm}} = 0 \tag{5}$$

where $k_{zm} = \sqrt{k_0^2 - k_x^2 - k_{ym}^2}$.

The dispersion equation can be solved approximately using a first-order Newton method, with a procedure similar to the one used in [12]. Fig. 3 shows the results of the dispersion analysis in the portion of the complex plane $-k_0 < \mathrm{Re}[k_x] < k_0$ and $-k_0 < \mathrm{Im}[k_x] < k_0$. The continuous curves, as a function of the slots widths w_s and parameterized for different heights h_s of the antenna with respect to the backing reflector, indicate the location of pole singularities k_{xp}^{sl} of the GF. The array is characterized by $d_x = d_y = 0.5\lambda_0$, with $\lambda_0 = 2\pi/k_0$.

The poles represented in Fig. 3 are of the leaky wave type, in the sense that they are characterized by a propagation $\mathrm{Re}[k_{xp}^{sl}]$ and by an attenuation constant $\mathrm{Im}[k_{xp}^{sl}]$, this latter associated with radiation losses.

When the backing reflector is farther away from the radiating slots, the propagating mode of the slot k_{xp}^{sl} is quasi-TEM,

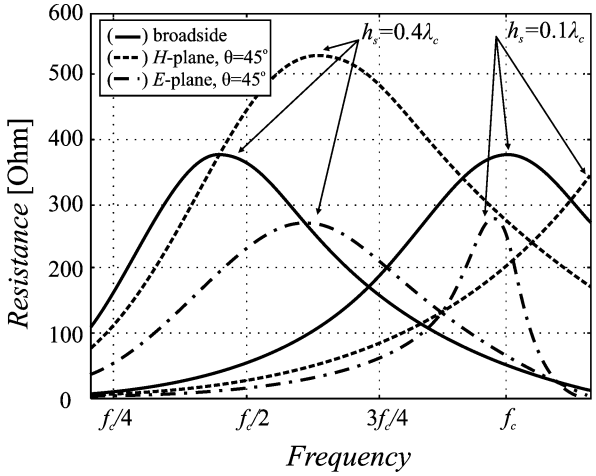

Fig. 4. Active impedance of a connected slot array as a function of the frequency for two heights.

traveling almost parallel to the slot direction. As h_s becomes smaller, the mode field distributions are much more affected by the presence of the backing reflector. As a consequence, the poles present an increasingly larger imaginary part. Most importantly, they present a smaller real part, meaning that they can be relevant also for arrays scanning in directions closer to broadside, since $\sin\theta = \mathrm{Re}(k_{xp}^{sl}/k_0)$. The propagation becomes more frequency dependent. An increasing width of the slots is also associated with an increased dispersivity. In fact, as the slot becomes wider, the field is less tightly bound to the slots, and the presence of the ground plane has more impact.

Curves similar to those in Fig. 3 have been obtained also for $\phi \neq 0$, i.e., scanning in planes different from the H-plane. However, since equivalent qualitative conclusions could have been obtained, they are not reported here. Lower values of h_s imply poles in the visible region of the k_x spectrum.

To highlight the negative effect due to the compatibility of connected slot arrays with leaky wave poles, Fig. 4 shows the real parts of the input impedance of a connected slot array, over a broad frequency range. Named λ_c the wavelength at the desired maximum operating frequency, the curves are given for $h_s = 0.1\lambda_c$ and $h_s = 0.4\lambda_c$. The remaining array parameters are fixed at $w_s = 0.2\lambda_c$, $d_x = d_y = 0.5\lambda_c$, and $\delta_s = 0.05\lambda_c$. The curves are also given for different scanning (broadside and 45° in the E- and H-planes). It is apparent that for smaller heights the resonances are indeed shifted toward higher frequencies. However, smaller heights imply the drastic narrowing of the useful band when scanning in the E-plane.

Given these findings, it is clear that reducing h_s to achieve matching at higher frequencies, and accordingly to reduce the number of T/R modules, it is not a viable solution since the scanning performances are seriously degraded.

B. TEM Poles in Connected Dipoles

If a similar dispersion analysis is performed for the connected dipole array, in the presence of a backing reflector, no leaky wave poles are found for h_d relatively small. This can be shown fairly easily. In the case of dipoles, one needs to find the solutions of the following dispersion equation, which is obtained equating to zero the denominator of the expression in (2):

$$\left(k_0^2 - k_{xm}^2\right) \sum_{m_y=-\infty}^{\infty} \frac{J_0\left(k_{ym}\frac{w_d}{2}\right)}{k_{zm}(1 - j\cot(k_{zm}h_d))} = 0. \quad (6)$$

Despite being similar to (5), the analytic solutions of (6) are simpler to characterize. Solutions are found explicitly, for arbitrary values of frequency, scanning angle ϕ, and distance from the ground plane h_d, in correspondence of $k_x = \pm k_0$. They are associated with guided microstrip-like (TEM) modes. Other poles emerge at higher frequencies. In fact, they arise from the reduced dispersion equation

$$\sum_{m_y=-\infty}^{\infty} \frac{J_0\left(k_{ym}\frac{w_d}{2}\right)}{k_{zm}(1 - j\cot(k_{zm}h_d))} = 0. \quad (7)$$

The possible solutions of this reduced dispersion equation are found observing that:

- $1 - j\cot(k_{zm}h_d) = 2/(1 - e^{-jk_{zm}2h_d})$;
- for a well-sampled radiating array, k_{zm} is always purely imaginary except in correspondence of $m_y = 0$, in which case $k_{z0} = k_0\cos\theta$;
- both real and imaginary parts of (7) must be zero in order to have a solution of the dispersion equation.

From the last two conditions, it follows that the contribution to the summation associated with the mode of index $m_y = 0$ must present a zero by itself. This is only possible when $(1 - e^{-jk_0\cos\theta 2h_d}) = 0$, which leads to $h_d = (n\lambda_0)/(2\cos\theta)$, where n is integer. Thus, the distance between the ground plane and the dipoles should be at least larger than half wavelength to have another pole, different from the microstrip TEM mode $(k_x = \pm k_0)$, to be compatible with the structure.

These microstrip-like TEM modes are important since they guide power from one feed to the next, but they do not imply important degradation of the main focused radiation, since they contribute to radiation toward $\theta \approx 90°$. Accordingly, the reduction of the height h_d does not present drawbacks specifically associated with scanning. However, a dipole array, whether connected, has a significantly reduced radiation BW when the h_d is small with respect to the wavelength. This can be observed in Fig. 5 where the real part of the impedances associated with two arrays of different heights but the same sampling are compared. Differently from the slot case, for the dipoles, we observe not only a shift of the resonance when varying the distance h_d from the ground plane, but also much higher impedance value for lower h_d. Here the growth of impedance is the manifestation of a transverse, nonradiating, resonance due to the mutual coupling between different dipoles.

Overall, one can conclude that the nature of the dominant waves in connected arrays of dipoles is much simpler (pure TEM) than the one (leaky) of connected arrays of slots. However, for neither structures, a lower height brings significant advantages.

IV. BW Dependence on the Gap Width

So far it has been established that the impedances of grounded connected dipoles and slots have similar dependencies on the periodicity and the distance from the ground plane. Where they

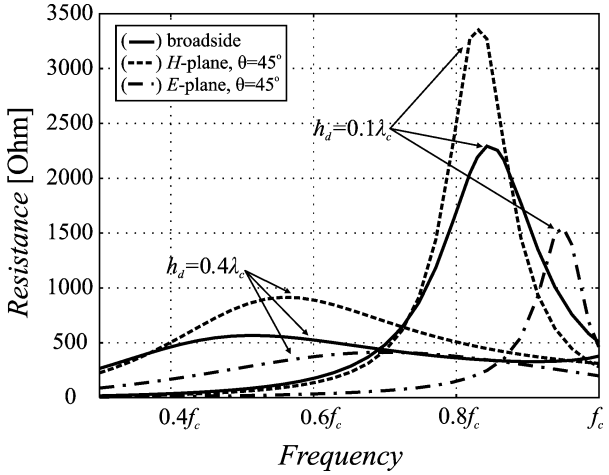

Fig. 5. Active impedance of a connected dipole array as a function of the frequency for two heights.

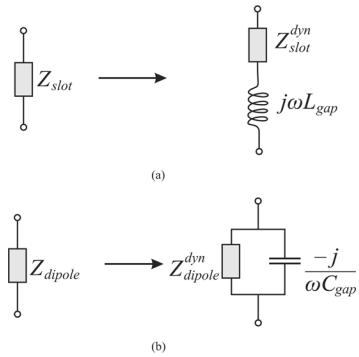

Fig. 6. Equivalent circuit representing the active impedance of each feed (a) of a connected array of slots with inductive gap feed and (b) of dipoles with capacitive gap feed.

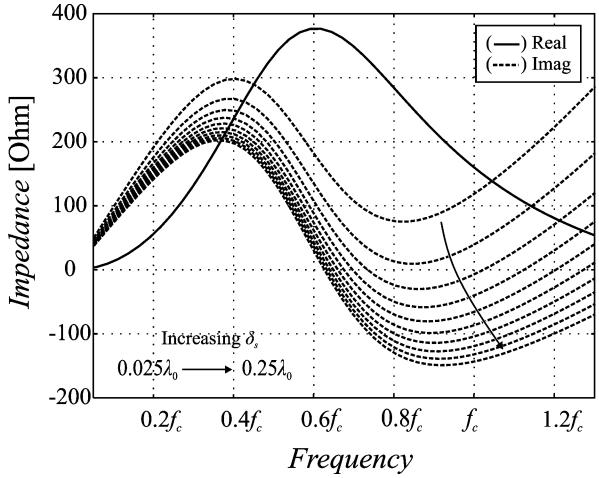

Fig. 7. Active impedance of a connected slot array as a function of the frequency for different gap widths, given $h_s = 0.3\lambda_c$, $w_s = 0.2\lambda_c$, and $d_x = d_y = 0.5\lambda_c$.

truly differ is in their dependence from the reactive energy stored in the feeding gaps. In the connected slot case, this reactive energy has only a marginal role, while in the case of connected dipoles, the reactive energy can be used to effectively achieve wider matching BWs.

The reactive energy is mathematically represented in the admittance of the connected dipoles (2) or in the impedance of the connected slots (1) by the higher order Floquet modes. This energy is localized in the proximity of each gap. Thus, for instance, in a connected slot array, one can assume that the concentrated inductance in each of the δ-gaps in every slot is the same as that localized in a single δ-gap of a unique infinitely extended slot etched on an equivalent ground plane in absence of the backing reflector. Analogously, one can assume that the concentrated capacitance associated with the δ-gaps in a connected dipole array is the same as that of a single feed of an infinite dipole. For the interested reader, these lumped equivalent impedances were provided in [18].

A. Slot Case: Lumped Inductance

In the connected slot array case, the lumped inductance associated with each feed gap is in series with respect to an equivalent circuit representing the excitation for the gap. That is because in a well-sampled array, the real part of the impedance is only associated with the dominant $(m_x = 0)$ term of the Floquet mode summation in (1). The imaginary part depends also on all the other additive modes in m_x. In Fig. 6(a), the equivalent circuit is shown, introducing the dynamic portion of the impedance as the difference between the input impedance and the concentrated inductive reactance associated with the gap. In order to highlight the effects of this inductance, Fig. 7 shows a parametric investigation of the input impedance as a function of the frequency for increasing dimension of the gap δ_s. It can be noted that the real part of the impedance is indeed not dependent on the dimension of the gap. At the lower frequencies, for all values of δ_s, the imaginary part of the impedance is inductive (positive). That is because the slots are operating in the close vicinity of the backing reflector, which acts as a short circuit [just considering the dominant Floquet wave representation in (3) is sufficient to verify this aspect]. Then, as the frequency grows, the waves reflected from the ground plane tend to add less destructively to the ones directly radiated toward free space, until a resonant condition is achieved. Eventually, the actual resonant condition, when the imaginary part of the input impedance is equal to zero, depends on the specific width of the δ-gap. It is apparent that for larger (less inductive) gaps the resonance occurs at slightly higher frequencies.

Note that the active input impedance cannot be seen as purely inductive, but only the reactive energy localized at the feeding points is modeled as an inductance.

B. Dipole Case: Lumped Capacitance

In the case of connected dipoles, the gaps can instead be truly used as a design parameter to enlarge the BW. Here a lumped capacitance representing the stored energy is in parallel with respect to the equivalent circuit of the excitation [see Fig. 6(b)]. That is because the capacitance is associated with the summation of the higher order contributions to the input admittance. Note that, in this case, in the equivalent circuit, the dynamic impedance $Z_{\rm dipole}^{\rm dyn}$ is equal to $1/Y_{\rm dipole}^{\rm dyn}$, where the dynamic admittance $Y_{\rm dipole}^{\rm dyn}$ is the difference between the input admittance and the spectrally capacitive susceptance. If the array is densely sampled, the real part of the admittance is associated with the $m_x = 0$ mode only, while the imaginary part depends also on

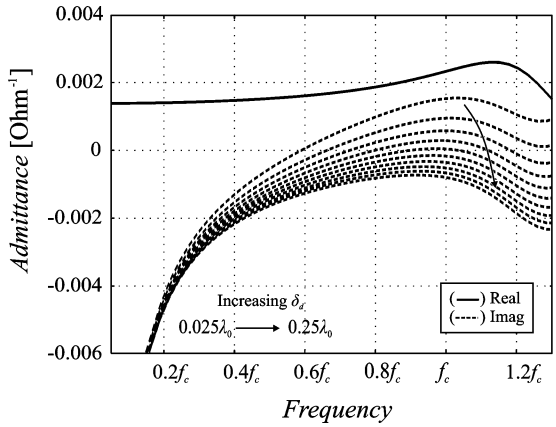

Fig. 8. Active admittance of a connected dipole array as a function of the frequency for different gap widths, given $h_d = 0.3\lambda_c$, $w_d = 0.05\lambda_c$, and $d_x = d_y = 0.5\lambda_c$.

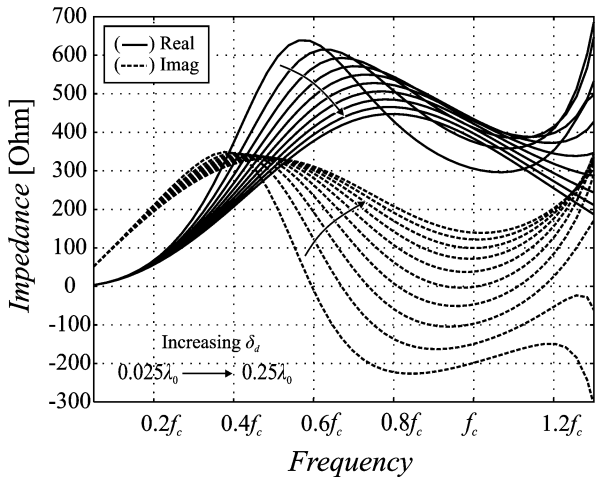

Fig. 9. Active impedance of a connected dipole array as a function of the frequency for different gap widths, given $h_d = 0.3\lambda_c$, $w_d = 0.05\lambda_c$, and $d_x = d_y = 0.5\lambda_c$.

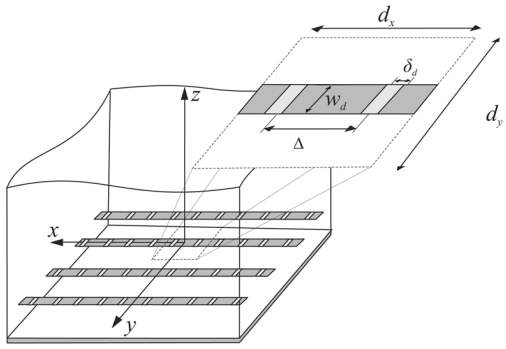

Fig. 10. Schematic geometry of a double-feed configuration that guarantees low feed capacitance despite that the width of each of the δ-gap is maintained small.

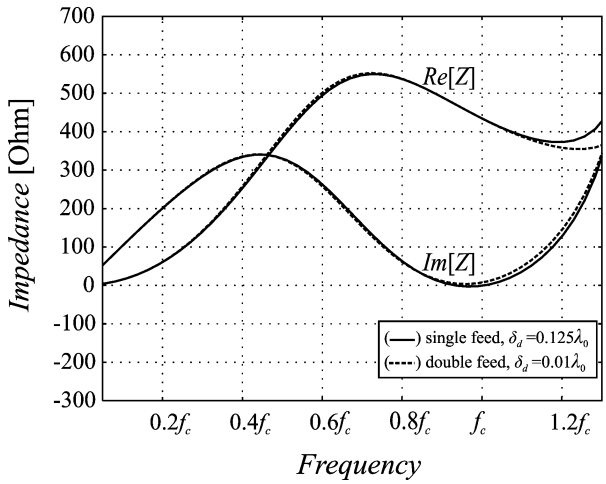

Fig. 11. Real and imaginary part of the active impedance of a connected dipole with single feed ($\delta_d = 0.125\lambda_0$), and with double feed ($\Delta = 0.29\lambda_0, \delta_d = 0.01\lambda_0$).

higher order modes. In Fig. 8, parametric curves of the input admittance as a function of the frequency are shown, for increasing dimension of the gap δ_d. The susceptance is inductive (< 0) for all the values of δ_d at the lower frequencies, when the dipoles are very close to the ground plane (short circuit). For higher frequencies, resonant conditions are achieved in different frequency points, depending on the specific width of the δ-gap. Let us observe the correspondent input impedance curves, shown in Fig. 9: when the gaps are small and the stored capacitive energy is high, the curves associated with the real part of the impedance define a relatively narrow bell as in the connected slot array case (Fig. 7). However, when the dimensions of the gaps are nonnegligible with respect to the wavelength, and accordingly, the gaps store less capacitive energy, the overall impedance bell appears lower, much wider, and shifted toward higher frequencies. The same effect is not present in the slot case, where the series inductance would not affect the real part of the impedance. Thus, we can already see that the gaps capacitance is a key design parameter that can be tuned to obtain wider matching BW of the connected dipole array.

The nicest aspect about this design parameter is that it allows to enlarge the impedance bells independently from the scanning angle to which the array is pointing. It is thus apparent that, when interested in broad BW and wide angle scanning, one should aim at a configuration which implements this controlled capacity condition.

V. Double Feed for the Dipoles

From the curves in Fig. 9, it appears that the best matching would be achieved for $\delta_d = 0.15\lambda_0$. However, the practical realization of such large gaps is not simple, since it would require feeding lines (for instance, coplanar strip lines) with interconductor distances so large that they would start radiating strongly cross-polarized fields. The solution that we envisage is to excite a connected array of dipoles with a double feed in each periodic cell. The schematic view of the feeding arrangement is shown in Fig. 10. In this case, the effective capacitance at each cell is essentially divided by two, since the two feeds are connected in series. It is clear that, due to the logarithmic dependence of the capacitance from the gap width [18], much narrower gaps can be used in the double-feed case to obtain similar impedance curves, with respect to the single-feed configuration. With such small gaps, the dipoles can be fed by transmission lines with negligible losses for cross-polar radiation. Fig. 11 shows the comparison between the input impedances in the two cases of single feed with $\delta_d = 0.125\lambda_0$, and double feed

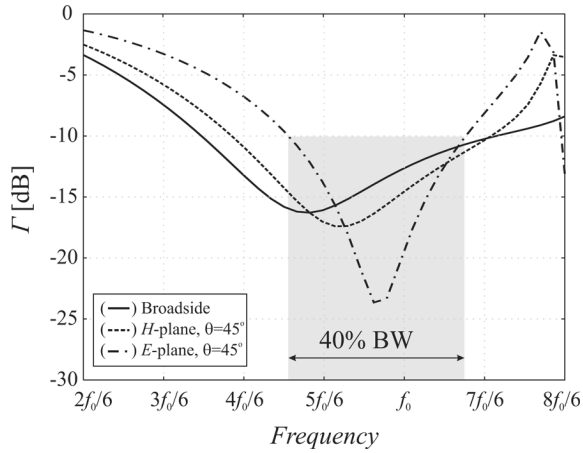

Fig. 12. Active reflection coefficients, with respect to 350 Ω of a dipole array characterized by $d_x = d_y = 0.45\lambda_0$, $w_d = 0.05\lambda_0$, $\delta_d = 0.01\lambda_0$, $\Delta = 0.29\lambda_0$, and $h_d = 0.31\lambda_0$. Curves are shown for scanning at broadside and toward $\theta = 45°$ in the two main planes.

with $\delta_d = 0.01\lambda_0$. An optimized array configuration based on a double feed per each unit cell was found to have 40% relative BW, scanning up to 45°, as show in Fig. 12. The feeds are at a distance $\Delta = 0.29\lambda_0$, the gap size δ_d is chosen equal to $0.01\lambda_0$, the dipole width is $w_d = 0.05\lambda_0$, and the height from the ground plane is $h_d = 0.31\lambda_0$. In order to simplify the analysis with only minimal loss of generality, the double-feed curves in Figs. 11 and in 12 have been obtained representing the double-feed configuration by two delta gap generators in each cell. Then, the cell input impedance is the sum of two equal feed impedances, each of them defined as the inverse of the average active admittance observed at the two ports. The description, the meaning, and the mathematical representation of this implementation are discussed in the next section.

A. Active Admittance for Multiple Feeds Per Unit Cell

The excitation of two feeding points can be modeled as two impressed electric fields $e_{1,2}(x)$, such as to create a voltage drop of 0.5 V at each feed. Assuming that the separation between the two feed points inside the same cell is Δ, the x-dependence of the electric field can be expressed as

$$e_{1,2}(x) = \frac{1}{\delta_d}\Pi_{\delta_d}\left(x \pm \frac{\Delta}{2}\right)$$

where

$$\Pi_{\delta_d}(x) = \begin{cases} 1, & \text{if } x \in \left[-\dfrac{\delta_d}{2}, \dfrac{\delta_d}{2}\right] \\ 0, & \text{otherwise.} \end{cases} \tag{8}$$

Accordingly, the Fourier transform (FT) of the entire impressed electric field on the cell is

$$\begin{aligned} E(k_x) &= \int_{-\frac{\delta_d}{2}-\frac{\Delta}{2}}^{\frac{\delta_d}{2}-\frac{\Delta}{2}} e_1(x')e^{jk_x x'}dx' + \int_{-\frac{\delta_d}{2}+\frac{\Delta}{2}}^{\frac{\delta_d}{2}+\frac{\Delta}{2}} e_2(x')e^{jk_x x'}dx' \\ &= 2\cos\left(k_x\frac{\Delta}{2}\right)\operatorname{sinc}\left(k_x\frac{\delta_d}{2}\right). \end{aligned} \tag{9}$$

In a 2-D periodic array, following the same procedure as in [11], the current distribution along the dipole associated with the excitation in (8) can be written as

$$i(x) = \frac{k_0 d_y}{\zeta_0 d_x}\sum_{m_x=-\infty}^{\infty} 2\cos\left(\frac{k_{xm}\Delta}{2}\right)\operatorname{sinc}\left(\frac{k_{xm}\delta_d}{2}\right) \cdot \frac{e^{-jk_{xm}x}}{(k_0^2 - k_{xm}^2)\displaystyle\sum_{m_y=-\infty}^{\infty}\frac{J_0\left(k_{ym}\frac{w_d}{2}\right)}{k_{zm}(1 - j\cot(k_{zm}h_d))}}. \tag{10}$$

Proceedings in duality with what was shown in [19], the admittance in a gap feed of a dipole excited by unitary impressed voltage drop can be calculated as the average electric current flowing in the gap. Accordingly, the active admittance in each of the two feeds can be expressed as

$$y_{1,2} = \frac{1}{\delta_d}\int_{-\frac{\delta_d}{2}\mp\frac{\Delta}{2}}^{\frac{\delta_d}{2}\mp\frac{\Delta}{2}} i(x')dx'. \tag{11}$$

Substituting (10) in (11), and performing the integration in the x'-variable, we obtain

$$y_{1,2} = \frac{k_0 d_y}{\zeta_0 d_x}\sum_{m_x=-\infty}^{\infty} 2\cos\left(\frac{k_{xm}\Delta}{2}\right)\operatorname{sinc}^2\left(\frac{k_{xm}\delta_d}{2}\right) \cdot \frac{e^{\pm jk_{xm}\frac{\Delta}{2}}}{(k_0^2 - k_{xm}^2)\displaystyle\sum_{m_y=-\infty}^{\infty}\frac{J_0\left(k_{ym}\frac{w_d}{2}\right)}{k_{zm}(1 - j\cot(k_{zm}h_d))}}. \tag{12}$$

By comparing (12) with (2), it is apparent that, for a well-sampled array in which only the $m_x = m_y = 0$ mode is dominant, the admittance at each feed point, in this double-feed configuration, is twice as large as the admittance of the same array with a single feed per cell. As a result, within this approximation, the input impedance at each of the two feeds roughly becomes half the single-feed value. Only when the two ports are connected in series, the single-feed value is approximately recovered.

In practice, when the cell is fed at two points which are physically separated, the maintenance of a voltage excitation at the same amplitude and phase for the two ports can be achieved by means transmission lines that implement a series feeding scheme, as shown in Fig. 13. In that case, the active input admittance at the section AA' cannot be evaluated without introducing an explicit phase shift.

However, it might be convenient and useful to refer to the concept of the average input admittance $y_{\text{in}}^{\text{av}}$ for each feed, which is defined as

$$\begin{aligned} y_{\text{in}}^{\text{av}} &= \frac{y_1 + y_2}{2} \\ &= \frac{k_0 d_y}{\zeta_0 d_x}\sum_{m_x=-\infty}^{\infty} 2\cos^2\left(\frac{k_{xm}\Delta}{2}\right)\operatorname{sinc}^2\left(\frac{k_{xm}\delta_d}{2}\right) \\ &\quad \cdot \frac{1}{(k_0^2 - k_{xm}^2)\displaystyle\sum_{m_y=-\infty}^{\infty}\frac{J_0\left(k_{ym}\frac{w_d}{2}\right)}{k_{zm}(1 - j\cot(k_{zm}h_d))}} \end{aligned} \tag{13}$$

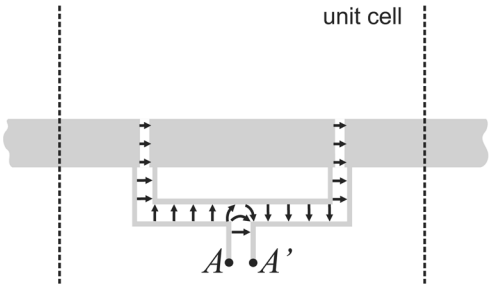

Fig. 13. Schematic representation of the double-feed excitation in a unit cell and related electric field vector lines.

and consequently, the average input impedance of each feed in a double cell is $z_{\rm in}^{\rm av} = (1)/(y_{\rm in}^{\rm av})$.

Finally, the cell input impedance is $z_{\rm cell} = 2z_{\rm in}^{\rm av}$. This is the impedance plotted in dashed lines in Fig. 11 and to which Fig. 12 refers.

Since for broadside radiation, the double-feed structure is actually a practical implementation of a feed sampling twice as dense, one might think that it is simply the effect of the denser sampling that helps the matching. However, this is only partly true. In fact, when the array is phased to scan, the two feed points are associated with the same phase shifting. The practical realization of such a double feed, similar to the one in [14], requires the connection of the two feeds via an appropriate transmission line, as shown in Fig. 13.

B. Practical Considerations

This final configuration that includes the double feed represents a schematic design, without explicit feeding network, that has been taken as baseline for the development of a prototype demonstrator that is presently being manufactured [20] in the framework of a contract with the European Space Agency.

For the practical realization of the feeding network in a connected array, it is important to note that differential lines also support common mode propagation. This latter, while unwanted, is always present. A detailed representation of the effects of common mode resonances in connected arrays has been recently discussed in [21]. The authors of this paper have also encountered such resonances in their designs and different strategies are being investigated to overcome the problems associated with them. The strategies depending on the specific applications may range from proper balun designs to the use of differential amplifiers very close to the radiating elements. This specific problem will be the object of follow-up contributions, focusing on the implementations rather than the general theory of connected arrays.

VI. Active Array Far-Field Patterns

The single most important reason for developing phased arrays based on connected dipoles or slots is the possibility to obtain radiation patterns of the highest polarization purity for wide scanning angles and over large frequency bands. Using the present GF formalism, the radiation patterns can be evaluated analytically, which not only saves computational design time, but eventually rigorously demonstrates the polarization purity properties of these arrays.

Before proceeding to the derivation of the radiated fields, it is worth noting that in this section, we will focus on *active far fields* radiated by *active currents*. This means that, as typically done in large phased arrays, the radiating currents are those present when all feeds are excited with ideal, uniform amplitude, impressed voltages (electric field). In reality, one can only use real generators. Thus, the realization of a feeding network that implements such uniform voltage generators independently from the scan angle and the frequency must be properly designed and it could turn out to be very challenging, particularly, more so in the present case of connected arrays, for which the mutual coupling between the elements is very high. The practical realization of a connected dipole array prototype will be the subject of a separate investigation. For the present time, we will make use of the *active current* ideal model.

The electric far field can be simply obtained from the expression of the electric potential and in particular

$$E_\theta = -j\omega \cos\theta \cos\phi A_x \tag{14}$$

$$E_\phi = j\omega \sin\phi A_x. \tag{15}$$

After a few algebraic manipulations, it can be shown that the potential in the far field can be expressed analytically as

$$A_x(\mathbf{r}) = \frac{\mu}{4\pi}\frac{e^{-jk_0 r}}{r}(1 - e^{-jk_0 2h_d \cos\theta}) \cdot J_x(k_0 \sin\theta\cos\phi, k_0 \sin\theta \sin\phi) \tag{16}$$

where $J_x(k_x, k_y)$ is the FT of the electric current distribution on the array. The key step in the evaluation of the far field is the approximation of the equivalent currents on the finite array. $J_x(k_y, k_y)$ can be expressed as the product of two separate variables, i.e., $J_x(k_y, k_y) = J_x^y(k_y)I(k_x)$.

Windowing approach [16] can be safely used in approximating the current distribution transverse to the array $J_x^y(k_y)$. For N_y elements along the transverse direction, remembering that in each dipole the distribution verifies the edge singular condition, it results

$$J_x^y(k_y) = AF(k_y - k_{y0}, N_y, d_y) J_0\left(\frac{1}{2} w_d k_y\right) \tag{17}$$

where $AF(k_y - k_{y0}, N_y, d_y) = \sum_{n_y=-N_y/2}^{N_y/2} I_{n_y} e^{j(k_y - k_{y0})n_y d_y}$.

The longitudinal direction is instead more critical. In fact, in Section III, we have demonstrated analytically that in any connected array, slots, or dipoles, a dominant propagating mode is supported by the structure with backing reflector, even at low frequencies. This mode is a leaky wave in the slot case or a bounded microstrip mode in a connected dipole array. In particular, in the dipole case, the waves traveling from the edges in the longitudinal direction $\pm\mathbf{i}_x$ are not attenuated. This suggests that an infinite-array approximation could be much less accurate as it completely neglects longitudinal standing waves and associated heavy current tapering that could exist even in the presence of uniform excitations.

The complication in the analysis is only apparent since we have actually provided the analytical closed-form expression for the GF of an infinitely extended dipole (or slot) in the spectral domain (see the Appendix), from which one can extract

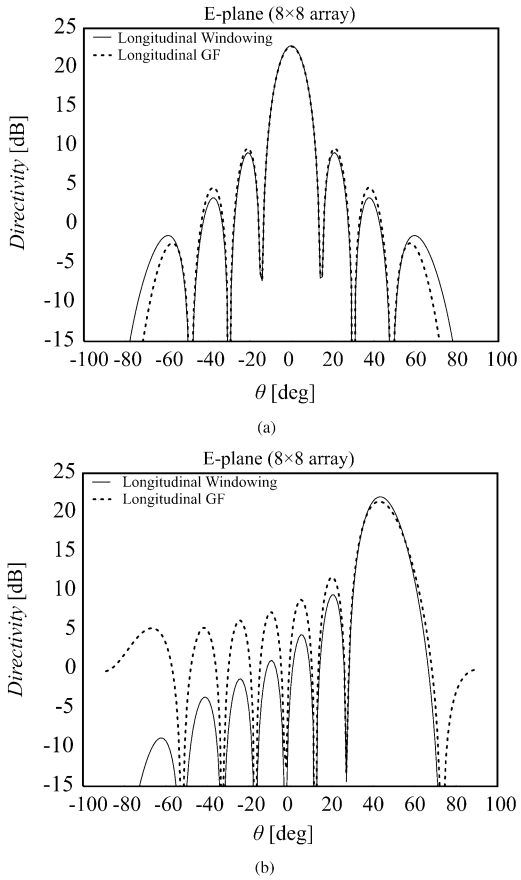

Fig. 14. Active array patterns from an 8×8 connected dipole array as in Fig. 12, Comparison between longitudinal windowing and longitudinal GF approach when (a) scanning broadside and (b) at elevations of 45° in the E-plane.

the spectrum of the longitudinal current in the case of a finite number of δ-gap sources

$$I(k_x) = V_0 AF(k_x - k_{x0}, N_x, d_x) \cdot \frac{\mathrm{sinc}(k_x \delta_d/2)}{D_\infty(k_x)}. \quad (18)$$

This expression based on the exact GF is more accurate than those achieved using a windowing approximation and it also implies reduced computational cost.

The far-field copolar directivity patterns radiated by an array of eight dipoles each one of them fed by eight δ-gap feeds is then investigated. The chosen frequency is $f_0 = c_0/\lambda_0$, where c_0 is the free-space speed of light. The array dimensions in terms of the wavelength are $d_x = d_y = 0.5\lambda_0$, $t = w_d = 0.05\lambda_0$, and $h_d = 0.31\lambda_0$.

In Fig. 14, we compared the E-plane radiation patterns obtained with the windowing approximation and the exact GF in (18). When observing in the E-plane, broadside, or at scanning, the use of the complete GF shows higher sidelobe levels and also broader beams at 45°. The use of the GF predicts also higher radiation at grazing angles. The actual values of grazing radiation are not very significant, since they will be eventually affected by the finite length of the dipoles, however their visibility suggests the necessity to control endpoint longitudinal radiation when dealing with connected arrays of small dimension.

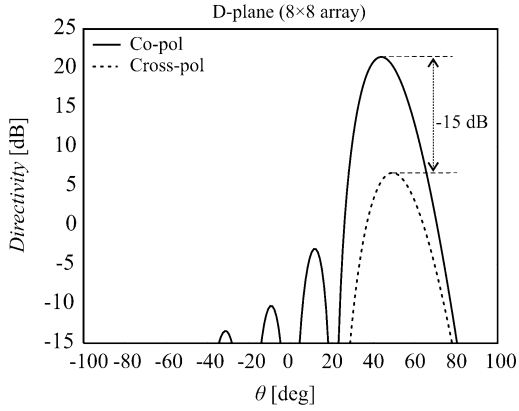

Fig. 15. Copolarized and cross-polarized directivities in the diagonal plane $\phi = 45°$ as a function of the elevation angle θ. The fields are again those radiated from an 8×8 connected dipole array as in Fig. 12.

Finally, Fig. 15 presents a comparison between the copolar and the cross-polar directivity obtained when the array is scanned to $\theta = 45°$ in the diagonal plane, $\phi = 45°$. The third Ludwig definition has been used [22]. The cross-polarized field is at least 15 dB lower than the copolarized field. This level of low cross polarization is the same of a single elementary dipole operating in free space and thus the value theoretically achievable by planar array of linearly polarized dipoles.

VII. Conclusion

Based on rigorous GF formulations, a comparison between the performances in scanning of connected arrays of dipoles and slots in the presence of a backing reflector is shown. The investigation reveals that the reactive energy contained in the feeds of the connected dipoles can be tuned in order to achieve broadband matching, independently from the scan angle. Eventually, the case of a planar connected array of dipoles that presents the lowest theoretical cross-polarization levels for a planar array on a 40% BW even when scanning in elevation to 45° is presented. The number of required T/R modules remains limited with $0.5\lambda_0$ samplings at the highest operational frequency. The use of the rigorous GF in the prediction of the far fields in the E-plane provides more accurate results with respect to a standard windowing technique and is even less computationally intensive. The significance of the *active* patterns will be discussed and validated in a following paper that will include also the design of a prototype demonstrator.

Appendix
Green's Function of a Connected Dipole Array With a Backing Reflector

The derivation of the GF of an infinitely long dipole fed by a single δ-type gap source is summarized here. The procedure is a simple extension of the one shown for the slot case in [12], to which the reader is referred to for a more in depth derivation; the extension to arrays of dipoles is also straightforward, similarly to what was presented in [11]. The canonical geometry and the pertinent reference system considered here is depicted in Fig. 16. An infinitely long dipole of width w_d, directed along x is

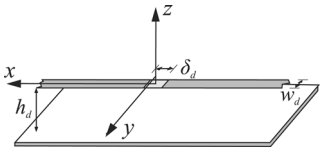

Fig. 16. Geometry of a single infinitely extended dipole with backing reflector excited at its center by a δ-gap generator.

located in the $x-y$ plane at distance h_d from an infinite backing reflector. The dipole is fed by an x-directed electric field at its origin (uniformly distributed along w_d).

A separable functional dependence for the transverse (across the dipole) and longitudinal electric current distribution is assumed, i.e., $j(x', y') = i(x') \cdot j_t(y')$. The transverse y-dependence of the electric current in the dipole is required to satisfy the quasi-static edge singularities $j_t(y') = (2)/(w_d\pi)(1 - (2y'/w_d)^2)^{-1/2}$, where the normalization constant $2/(w_d\pi)$ has been chosen in such a way that $i(x')$ represents a net current flow along the dipole at any point x'.

The current along the entire dipole can be expressed as an inverse Fourier transform

$$i(x) = \frac{1}{2\pi} \int_{-\infty}^{\infty} \frac{-V_e(k_x)}{D(k_x)} e^{-jk_x x} dk_x. \tag{19}$$

In (19), the numerator V_e represents the FT of the impressed electric field distribution along x. In the present case, a δ-gap generator is considered, thus $V_e = V_0 \mathrm{sinc}(k_x\delta_d/2)$. The denominator is given by the convolution between the GF in absence of the dipole and the transverse electric current distribution. The denominator is expressed in the spectral domain as

$$D(k_x) = \frac{1}{2\pi} \int_{-\infty}^{\infty} G_{xx}(k_x, k_y) J_t(k_y) dk_y \tag{20}$$

where $J_t(k_y) = \mathrm{FT}\{j_t(y')\} = J_0(k_y(w_d/2))$ is the FT of transverse electric current with J_0 being the Bessel function of zeroth order. Also in (20), G_{xx} is the FT of the GF of the electric field parallel to the dipole, in the x-direction, radiated by the equivalent electric current replacing the dipole and its image in $z = -2h_d$.

Substituting in (20) the explicit GF, we obtain

$$D(k_x) = \frac{-\zeta_0}{4\pi k_0} \int_{-\infty}^{\infty} \frac{k_0^2 - k_x^2}{k_z} (1 - e^{-2jk_z h_d}) J_0\left(k_y \frac{w_d}{2}\right) dk_y \tag{21}$$

where $k_z = \sqrt{k_0^2 - k_x^2 - k_y^2}$ with $\mathrm{Im}[k_z] < 0$.

Substituting (21) in (19), the explicit double integral representation of the current in the infinitely long dipole can be obtained. For the rest of this paper, there is no interest in evaluating these integrals analytically, since only the double spectral summations arising from the periodic extensions are discussed in the text.

REFERENCES

[1] D. H. Schaubert, A. van Ardenne, and C. Craeye, "The square kilometer array (SKA) antenna," in *Proc. IEEE Int. Symp. Phased Array Syst. Technol.*, Oct. 2003, pp. 351–358.

[2] B. Swinyard, T. Nakagawa, H. Matsuhara, D. Griffin, M. Ferlet, P. Eccleston, A. di Giorgio, J. Baselmans, J. Goicoechea, K. Isaak, P. Mauskopf, L. Rodriguez, F. Pinsard, W. Raab, L. Duband, N. Luchier, N. Rando, A. Heras, T. Jagemann, N. Geis, and S. Vives, "The European contribution to the SPICA mission," *Proc. SPIE*, vol. 7010, no. 70100I, Jun. 2008, DOI:10.1117/12.789195.

[3] N. Inagaki, Y. Isogai, and Y. Mushiake, "Ichimatsu Moyou antenna—Self-complementary antenna with periodic feeding points," *Trans. IECE Jpn.*, vol. 62-B, pp. 388–395, Apr. 1979.

[4] C. E. Baum, "Some characteristics of planar distributed sources for radiating transient pulses," AFWL, Albuquerque, NW, Sens. Simulat. Note 100, Mar. 12, 1970.

[5] R. C. Hansen, "Linear connected arrays," *IEEE Antennas Wireless Propag. Lett.*, vol. 3, pp. 154–156, 2004.

[6] R. C. Hansen, "Non-Foster and connected planar arrays," *Radio Sci.*, vol. 39, no. RS4004, Jul. 2004, DOI:10.1029/2004RS003043.

[7] B. A. Munk, *Finite Antenna Arrays and FSS*. New York: Wiley, 2003, ch. 6, pp. 181–213.

[8] H. Wheeler, "Simple relations derived from a phased array antenna made of an infinite current sheet," *IEEE Trans. Antennas Propag.*, vol. AP-13, no. 4, pp. 506–514, Jul. 1965.

[9] J. J. Lee, S. Livingstone, and R. Koenig, "Wide band slot array antennas," in *Proc. Antennas Propag. Soc. Symp.*, Columbus, OH, Jun. 2003, vol. 2, pp. 452–455.

[10] A. Neto and J. J. Lee, "Infinite bandwidth long slot array," *IEEE Antennas Wireless Propag. Lett.*, vol. 4, pp. 75–78, 2005.

[11] A. Neto and J. J. Lee, "Ultrawide-band properties of long slot arrays," *IEEE Trans. Antennas Propag.*, vol. 54, no. 2, pp. 534–543, Feb. 2006.

[12] A. Neto and S. Maci, "Green's function of an infinite slot printed between two homogeneous dieletrics. Part I: Magnetic currents," *IEEE Trans. Antennas Propag.*, vol. 51, no. 7, pp. 1572–1581, Jul. 2003.

[13] B. Tomasic, N. Herscovici, and H. Steyskal, "Analysis of periodic array of infinitely-long slots fed by connected dipoles," in *Proc IEEE Antennas Propag. Symp.*, San Diego, CA, Jul. 5–12, 2008, pp. 1–4.

[14] J. J. Lee, S. Livingston, R. Koenig, D. Nagata, and L. L. Lai, "Compact light weight UHF arrays using long slot apertures," *IEEE Trans. Antennas Propag.*, vol. 54, no. 7, pp. 2009–2015, Jul. 2006.

[15] N. Amitay, V. Galindo, and C. P. Wu, *Theory and Analysis of Phased Array Antennas*. New York: Wiley, 1972.

[16] A. Ishimaru, R. J. Coe, G. E. Miller, and W. P. Geren, "Finite periodic approach to large scanning array problems," *IEEE Trans. Antennas Propag.*, vol. AP–33, no. 11, pp. 1213–1220, Nov. 1985.

[17] B. Munk, R. Taylor, T. Durharn, W. Croswell, B. Pigon, R. Boozer, S. Brown, M. Jones, J. Pryor, S. Ortiz, J. Rawnick, K. Krebs, M. Vanstrum, G. Gothard, and D. Wiebelt, "A low profile broad band phased array antenna," in *Proc. Antennas Propag. Soc. Symposium*, Columbus, OH, Jun. 2003, vol. 2, pp. 448–451.

[18] P. Focardi, A. Neto, and R. McGrath, "Coplanar waveguide based, terahertz hot electron bolometer mixers: Improved embedding circuit description," *IEEE Trans. Microw. Theory Tech.*, vol. 50, no. 10, pp. 2374–2383, Oct. 2002.

[19] A. Neto and S. Maci, "Input impedance of slots printed between two dielectric media and fed by a small Δ-gap," *IEEE Antennas Wireless Propag. Lett.*, vol. 3, pp. 113–116, 2004.

[20] D. Cavallo, A. Neto, G. Gerini, and G. Toso, "On the potentials of connected array technology for wide band, wide scanning, dual polarized applications," in *Proc. 30th ESA Antenna Workshop*, Noordwijk, The Netherlands, May 27–30, 2008, pp. 407–410.

[21] S. G. Hay, J. , and D. O'Sullivan, "Analysis of common-mode effects in a dual-polarized planar connected-array antenna," *Radio Sci.*, vol. 43, no. RS6S04, Dec. 2008, DOI:10.1029/2007RS003798.

[22] A. C. Ludwig, "The definition of cross polarization," *IEEE Trans. Antennas Propag.*, vol. AP-21, no. 1, pp. 116–119, Jan. 1973.

Andrea Neto (M'00) received the Laurea degree (*summa cum laude*) in electronic engineering from the University of Florence, Florence, Italy, in 1994 and the Ph.D. degree in electromagnetics from the University of Siena, Siena, Italy, in 2000. Part of his Ph.D. was developed at the European Space Agency Research and Technology Center, Noordwijk, The Netherlands, where he worked for the antenna section for over two years.

In 2000–2001, he was a Postdoctoral Researcher at California Institute of Technology, Pasadena, working for the Sub-mm Wave Advanced Technology Group. Since 2002, he has been a Senior Antenna Scientist at TNO Defence, Security and Safety, The Hague, The Netherlands. His research interests are in the analysis and design of antennas, with emphasis on arrays, dielectric lens antennas, wideband antennas, and EBG structures.

Dr. Neto was corecipient of the H.A. Wheeler award for the best applications paper of the year 2008 in the IEEE TRANSACTIONS ON ANTENNAS AND PROPAGATION. He presently serves as am Associate Editor of the IEEE ANTENNAS AND WIRELESS PROPAGATION LETTERS.

Daniele Cavallo (S'09) received the M.Sc. degree (*summa cum laude*) in telecommunication engineering from the University of Sannio, Benevento, Italy, in 2007. Currently, he is working towards the Ph.D. degree in the Telecommunication Technology and Electromagnetics group (TTE/EM), Eindhoven University of Technology, Eindhoven, The Netherlands.

Since January 2007, he has been with the Antenna Group at TNO Defence, Security and Safety, The Hague, The Netherlands. His research interests include the analysis and design of antennas, with emphasis on wideband phased arrays.

Mr. Cavallo was corecipient of the best innovative paper prize at the 30th ESA Antenna Workshop in 2008.

Giampiero Gerini (M'92–SM'08) received the M.Sc. (*summa cum laude*) and Ph.D. degrees in electronic engineering from the University of Ancona, Ancona, Italy, in 1988 and 1992, respectively.

From 1994 to 1997, he was a Research Fellow at the European Space Research and Technology Centre (ESA-ESTEC), Nooordwijk, The Netherlands, where he joined the Radio Frequency System Division. Since 1997, he has been with The Netherlands Organization for Applied Scientific Research (TNO), The Hague, The Netherlands. At TNO Defence, Security and Safety, he is currently Chief Senior Scientist of the Antenna Unit in the Transceivers and Real-Time Signal Processing Department. His main research interests are phased array antennas, frequency-selective surfaces, and integrated front ends. Since 2007, he has been also a part-time Professor at the Technical University of Eindhoven, Eindhoven, The Netherlands, where he holds a Chair on Novel Structures and Concepts for Advanced Antennas.

Dr. Gerini was corecipient of the H.A. Wheeler award for the best applications paper of the year 2008 in the IEEE TRANSACTIONS ON ANTENNAS AND PROPAGATION.

Giovanni Toso (S'93–M'00–SM'07) was born in La Spezia, Italy, on May 3, 1967. He received the Laurea (*summa cum laude*) and Ph.D. degrees in electrical engineering from the University of Florence, Florence, Italy, in 1992 and 1995, respectively.

In 1996, he was a Visiting Scientist at the Laboratoire d'Optique Electromagnétique, University of Aix-Marseille III, Marseille, France. From 1997 to 1999, he was a Postdoctoral student at the University of Florence. In 1999, he was a Visiting Scientist at the University of California at Los Angeles (UCLA) and received a scholarship from Thales Alenia Space (Rome, Italy). In 2000, he was appointed Researcher in a Radioastronomy Observatory of the Italian National Council of Researches (CNR). Since 2000, he has been with the Antenna and Submillimeter Section of the European Space and Technology Centre, European Space Agency, ESA ESTEC, Noordwijk, The Netherlands. His research interests are mainly in the field of array antennas for satellite applications and, in particular, in nonregular arrays, reflectarrays, and multibeam antennas. He has coauthored five patent applications, about 150 contributions to international conferences, peer-reviewed journals, and book chapters.

Dr. Toso is corecipient of the 2008 best paper prize at the 30th ESA Antenna Workshop. In 2009, he was coeditor of the Special Issue on Active Antennas for Satellite Applications published in the *International Journal of Antennas and Propagation*. His biography is included in the Marquis *Who's is Who in the World*.